nature climate change

ARTICLES

https://doi.org/10.1038/s41558-022-01455-w

Check for updates

Permafrost thaw drives surface water decline across lake-rich regions of the Arctic

Elizabeth E. Webb[1]✉, Anna K. Liljedahl[2], Jada A. Cordeiro[3], Michael M. Loranty[4], Chandi Witharana[5] and Jeremy W. Lichstein[3]

Lakes constitute 20–40% of Arctic lowlands, the largest surface water fraction of any terrestrial biome. These lakes provide crucial habitat for wildlife, supply water for remote Arctic communities and play an important role in carbon cycling and the regional energy balance. Recent evidence suggests that climate change is shifting these systems towards long-term wetting (lake formation or expansion) or drying. The net direction and cause of these shifts, however, are not well understood. Here, we present evidence for large-scale drying across lake-rich regions of the Arctic over the past two decades (2000–2021), a trend that is correlated with increases in annual air temperature and autumn rain. Given that increasing air temperatures and autumn rain promote permafrost thaw, our results indicate that permafrost thaw is leading to widespread surface water decline, challenging models that do not predict a net decrease in lake area until the mid-twenty-first or twenty-second centuries.

Air temperatures in the Arctic have warmed nearly 3 °C since the mid-1960s and at a rate more than twice the global average since 2000[1]. This warming has led to a myriad of changes to Arctic terrestrial ecosystems, including increasing precipitation[2–4], widespread permafrost thaw[5–9] and changes in surface water area[10,11]. Northern permafrost lands contain more lake area than any other region worldwide[12], and changes in the aerial extent of water have the potential to accelerate or mitigate feedbacks to regional and global climate[13–16]. Changes in surface water area, for instance, affect land surface albedo and account for ~10% of recent albedo-induced changes in radiative forcing in the continuous permafrost zone[13]. Permafrost thaw-induced changes in lake area also affect carbon cycling. Lake initiation and expansion increase carbon fluxes to the atmosphere because accelerated permafrost thaw beneath and around lakes unlocks previously frozen sediments for microbial decomposition[17,18]. Conversely, in drained lake basins, peat accumulation following vegetation regrowth and permafrost aggradation result in a net ecosystem carbon sink[19]. Models predict that with climate warming, permafrost thaw will result in greater lake expansion than drainage (a net increase in lake area) throughout the early to mid-twenty-first century[14,20], leading to a positive feedback to climate change[13,15,20].

Surface water change has been documented in analyses across the Arctic[10,21–23], with most studies showing surface water drainage in the discontinuous permafrost zone and both increasing and decreasing surface water trends in the continuous permafrost zone. These observations are fractured across space and time, however, with large portions of the permafrost zone unstudied. The limited spatial and temporal coverage of these site-level observations makes validating models difficult, especially since the direction of surface water change can vary by time period[24] and spatial scale considered[25]. Here, we (1) use satellite-derived data to report a spatially comprehensive and temporally consistent analysis of surface water change across lake-rich regions of the northern discontinuous and continuous permafrost zones over the past two decades (2000–2021), (2) identify the climate and landscape variables correlated with surface water change and (3) discuss the implications of surface water change for climate feedbacks.

Surface water trends across lake-rich regions of the Arctic

We used the Moderate Resolution Imaging Spectroradiometer (MODIS) satellite-based superfine water index (SWI)[26] to quantify surface water change across lake-rich regions of the Arctic over the past two decades (Fig. 1). SWI is a unitless water cover index that can track sub-pixel variations in surface water (SWI validation analysis in the Supplementary Information) and is positively correlated with percentage surface water cover[26]. In northern latitudes, a one unit increase in SWI is roughly equivalent to a 75% increase in surface water cover (SWI and percentage surface water cover conversion in the Supplementary Information).

Across the entire study region (areas of the northern discontinuous and continuous permafrost zones with at least 5% lake cover percentage), there was a decline in surface water over the past two decades (mean pixel-wise SWI trend of $-0.0009\,\mathrm{yr}^{-1}$), with 82% of 12 km pixels showing a negative trend (Fig. 1). The mean trends for discontinuous and continuous permafrost and for areas with and without thermokarst wetlands and lakes were also negative (Fig. 2 and Table 1). However, there was high spatial variability, with a substantial fraction of 500 m pixels having positive trends within each thermokarst land cover type (Table 1). Thus, at the 500 m pixel scale, there is high variability in surface water change (including both increases and decreases), but the net change over larger scales (for example, 12 km pixels in Fig. 1 or land cover types in Table 1) tends to be negative. This finding of widespread surface water decline corroborates recent work over more limited spatial scales showing enhanced drainage in the Arctic[5,27–29] but contradicts models of surface water dynamics used to quantify carbon emissions, which show rapid increases in surface water in the early to mid-twenty-first century[14,17,20].

Climate drivers

We used a machine learning model to determine the landscape and climate variables (from the ERA5-Land reanalysis dataset[30])

[1]School of Natural Resources and Environment, University of Florida, Gainesville, FL, USA. [2]Woodwell Climate Research Center, Falmouth, MA, USA. [3]Department of Biology, University of Florida, Gainesville, FL, USA. [4]Department of Geography, Colgate University, Hamilton, NY, USA. [5]Department of Natural Resources and the Environment, University of Connecticut, Storrs, CT, USA. ✉e-mail: webbe@ufl.edu

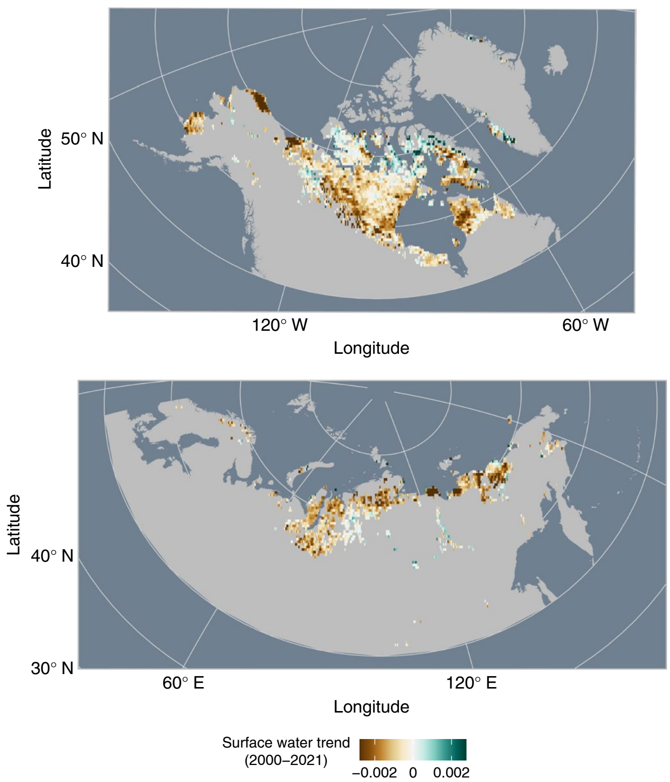

Fig. 1 | Change in the average July superfine water index (yr^{-1}) from 2000 to 2021. A change in SWI of −0.002 yr^{-1} corresponds to ~3% decrease in percentage surface water cover over 20 yr (for example, a change from 15 to 12% cover; 15% is the mean surface water cover across the study area). The study area includes areas of the continuous and discontinuous permafrost zones (Extended Data Fig. 4) where lake cover percentage is ≥5%. The continuous and discontinuous zones have an estimated permafrost percentage area of 90–100% and 50–90%, respectively[67]. Grey regions, which include areas where lake cover percentage is <5% and/or sporadic, isolated and non-permafrost zones, are not in the study area. Pixel resolution is 12 × 12 km^2.

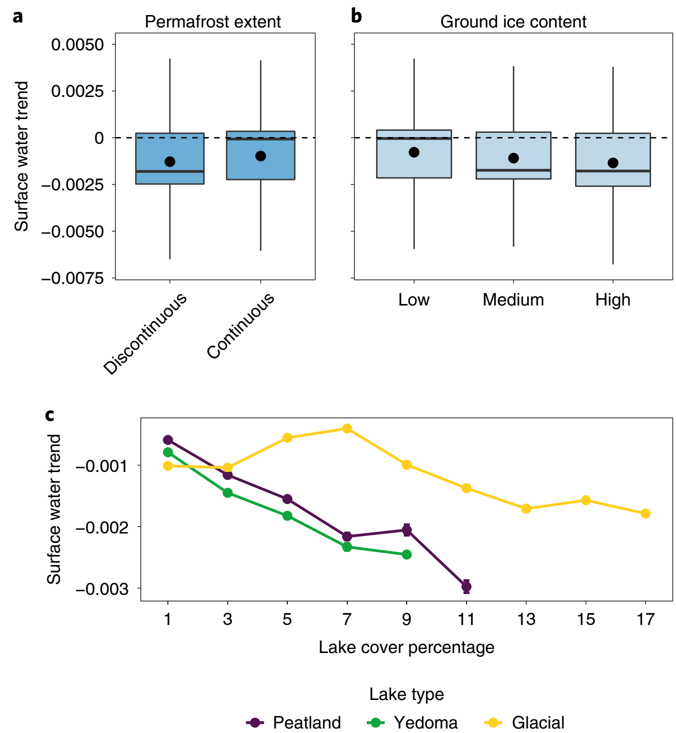

Fig. 2 | Pixel-wise surface water trends (change in the July SWI (yr^{-1}) from 2000 to 2021). a–c, Trends are binned by permafrost extent (**a**), ground ice content (**b**) and lake cover (percentage of the pixel area occupied by lakes) (**c**). Pixels in this figure (n = 22,216) are pixels whose surface water trends were in the lower/upper 20th/80th percentile of the 12 km pixels. Horizontal lines and circles in **a** and **b** represent the median and mean, respectively. Boxplot limits are the upper and lower quartiles, and whiskers are 1.5× the interquartile range. Surface water decreased more strongly in the discontinuous permafrost zone than in the continuous zone (P < 0.001, **a**) and more strongly in areas with high ice content than in areas with medium or low ice content (P < 0.001, **b**). Values in **c** are means (±s.e.) of 12 km pixels binned in 2% intervals with the x axis label representing the bin midpoints; bins containing <1% of the data were excluded. The surface water trend responds more strongly to increasing cover of yedoma and peatland lakes compared to glacial lakes (Supplementary Table 3). Peatland lakes have thick organic sediments and are mainly found adjacent to peatlands or in lowland tundra regions; yedoma lakes form in non-glaciated regions with yedoma deposits (organic-rich permafrost with high ice content); glacial lakes include all lakes with organic-poor sediments[62,68].

related to changes in surface water (from the MODIS-based SWI; Methods). Results from this analysis show that changes in annual air temperature and the amount of rain in the previous autumn (hereafter referred to as 'autumn rain') were the most important drivers of surface water change (Figs. 3 and 4). Both of these variables increased over the study period (Extended Data Fig. 1 and Table 2), and both had overall negative effects on surface water, although the relationships are not monotonic (Extended Data Fig. 2). These results suggest that, on average, increasing annual air temperature and increasing autumn rain both lead to decreasing surface water.

Increases in annual air temperatures, whether through gradual warming or more frequent heatwaves[31], could lead to decreasing surface water through two mechanisms: permafrost thaw or increased evapotranspiration. To test which process is primarily responsible, we included evapotranspiration in our machine learning model, and the results show that changes in evapotranspiration play a negligible role in surface water change across lake-rich areas of the Arctic (evapotranspiration was the most important driver in only 0.5% of the study area; Extended Data Fig. 3). Additionally, over our study area, the trend in annual precipitation (+1 mm yr^{-1}) was stronger than the trend in evapotranspiration (+0.6 mm yr^{-1}; Table 2), consistent with previous analyses[4,32] and in line with models that project a warmer and wetter Arctic[33]. Together these data suggest that the main mechanism through which increasing air temperatures has led to surface water declines is through new hydrological pathways caused by permafrost thaw rather than through a decrease in the precipitation–evapotranspiration balance.

Rain increased across the study region in the spring, summer and autumn (Table 2), reflecting both a gradual rise in warm season precipitation[4] as well as an increase in extreme precipitation events in recent years[34]. In the absence of permafrost thaw, increasing rain leads to increasing surface water. Thus, the negative relationship between autumn rain and surface water suggests that the primary effect of autumn rain on surface water is through permafrost thaw and not through the precipitation–evapotranspiration balance. Rain, particularly in the autumn, can increase soil temperature and thaw depth directly[35,36] through heat advection and indirectly because wetter soils have higher latent heat and therefore delay freeze-up in the autumn[37]. Extreme rainfall events can also destabilize permafrost terrain and accelerate thermoerosion[38,39], which promotes drainage channel formation[40]. Lastly, more rainfall can increase surface water

Table 1 | July surface water trends aggregated by thermokarst land cover type[66]

		Thermokarst wetlands[a]		Thermokarst lakes		Non-thermokarst areas
		High to very high	Low to moderate	High to very high	Low to moderate	
All pixels in land cover type	(%)[b]	19	65	26	21	16
	Trend	−0.0011 ± 0.0024	−0.001 ± 0.0028	−0.0013 ± 0.0025	−0.0007 ± 0.003	−0.0002 ± 0.0037
All extreme pixels in land cover type	(%)[b]	19	61	25	22	19
	Trend	−0.0015 ± 0.0037	−0.0012 ± 0.0045	−0.0019 ± 0.0038	−0.0006 ± 0.0045	0.0004 ± 0.0052
Top 20% of pixels in land cover type	(%)[c]	17	18	14	24	32
	Trend	0.0017 ± 0.0024	0.002 ± 0.0033	0.0017 ± 0.0025	0.0021 ± 0.0032	0.0029 ± 0.0039
Bottom 20% of pixels in land cover type	(%)[c]	23	20	24	18	16
	Trend	−0.0038 ± 0.0027	−0.0041 ± 0.0033	−0.004 ± 0.0027	−0.0041 ± 0.0035	−0.0045 ± 0.0037

[a]Wetland thermokarst landscapes include bogs, fens and shore fens. [b]Percentage of study region or extreme pixels found within each thermokarst land cover type. [c]Percentage of thermokarst land cover pixels with increasing/decreasing extreme surface water trends. Trends are the mean ± s.d. of the 500 m pixel-wise temporal trends in the SWI. The analysis reported in this table was performed at the scale of MODIS pixels (500 m), rather than aggregated 12 km pixels, to quantify fine-scale spatial variability in surface water trends. 'High to very high' and 'low to moderate' indicate fractional coverage of wetlands and lakes (high to very high: 30–100%; low to moderate: 1–30%). Rows sum to >100% due to partial overlap of thermokarst wetland and lake classifications (details in ref. [66] and Extended Data Fig. 4). The study region (n = 39,206,880 MODIS pixels) includes continuous and discontinuous permafrost land north of 50° N where lake cover percentage is ≥5%. Extreme pixels (n = 15,682,749) are those whose surface water trends were in the lower/upper 20th/80th percentile of the study region pixels.

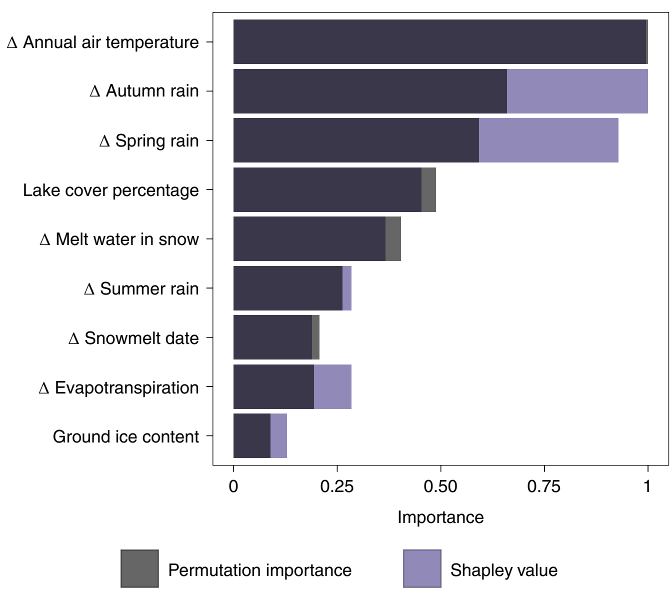

Fig. 3 | Relative importance of predictor variables in explaining surface water trends across the study region. Permutation importance and Shapley values are two different metrics of a variable's contribution to explained variation; both metrics identify changes in annual air temperature and autumn rain as the most important predictors of surface water change. The two methods are overlaid on each other; dark purple indicates overlap.

drainage by increasing lake levels and thereby accelerating mechanical and thermoerosion of drainage channels[29,41].

Our machine learning model performed better (higher R^2) when precipitation was partitioned seasonally rather than annually. Even though the trend in autumn rain was only ~70% of the magnitude of the trend in summer rain (Table 2), autumn rain explained more of the variation in surface water trends (Fig. 3). Together these results suggest that the timing of precipitation change is critical for predicting and understanding surface water trends in our study area. In the Arctic, autumn is a time of heat loss from the ground surface to the atmosphere, but unfrozen water in the soil at this time can result in ground surface temperatures up to 9 °C warmer during the month of freeze-up[37]. Thus, increasing autumn rain could extend the thawed season by weeks. Furthermore, unlike early season precipitation, which is lost to surface runoff because there is little infiltration into the frozen ground, autumn rain penetrates deeper into the active layer[42]. Thus, autumn rain will probably remain on the landscape until the spring, when it could combine with snowmelt to promote rapid lateral drainage channel development as lakes overtop their banks[27].

Landscape characteristics

Our machine learning analysis quantified the drivers of surface water change in 12 km pixels and may therefore underestimate the importance of landscape characteristics such as ground ice content and permafrost zone that are available only at coarser scales (Extended Data Fig. 4). Because of the known importance of these landscape variables to permafrost thaw-driven surface water change[11,14,43], we analysed ground ice content and permafrost zone separately from the finer-scale climate variables.

Surface water declined more strongly in the discontinuous permafrost zone of our study region than in the continuous permafrost zone (P < 0.001; Fig. 2), which is consistent with our understanding of how permafrost thaw drives landscape drainage. When present, permafrost prevents vertical and/or horizontal water flow. Permafrost loss increases hydrological connectivity by connecting adjacent terrain previously isolated by permafrost[44] or through talik formation (unfrozen ground otherwise surrounded by permafrost), which can increase surface water exchange with ground water[12,45–47]. Because discontinuous permafrost is thinner and less connected than continuous permafrost[48], temperature-driven permafrost loss and associated increasing hydrological connectivity is more likely in this zone. For example, talik formation is thought to have caused landscape-scale surface water drainage in discontinuous permafrost in Alaska[47] and Siberia[11] over recent decades.

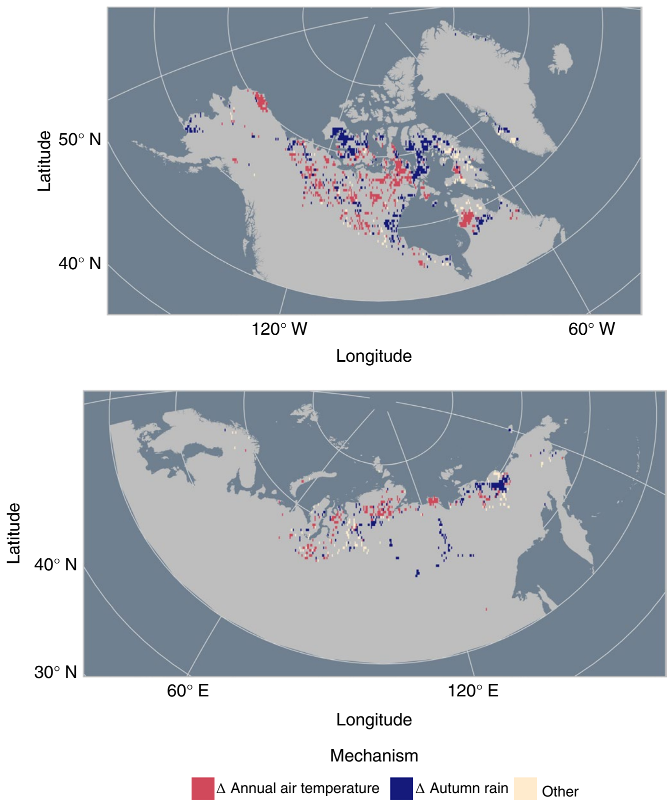

Fig. 4 | Predictor variables contributing the most to surface water trends in 12 km pixels, as determined using Shapley values. For each highlighted pixel, the effect on the surface water trend depends on both the sign and magnitude of the change in the predictor variable (Extended Data Figs. 1 and 2). Overall, the relationships between surface water trends and trends in annual air temperature and autumn rain are negative, but the relationships are not monotonic (Extended Data Fig. 2). This analysis includes pixels whose surface water trends were in the lower/upper 20th/80th percentile of all the 12 km pixels ($n = 22,216$). Extended Data Fig. 2 provides a map of 'other' mechanisms.

When ice-rich permafrost thaws, the land surface formerly sustained by ice can collapse and create ground subsidence. Water may pool in subsided areas, creating a new pond, which may expand laterally by thermoerosion at the lake margins[46]. Accordingly, models of surface water dynamics predict a net increase in thermokarst lake area (formation plus expansion minus drainage) until the mid- to late-twenty-first century (rates of thermokarst lake formation, expansion and drainage from ref. [20] are 0.3% yr^{-1}, 0.4% yr^{-1} and 0.03% yr^{-1}, respectively; net rate of thermokarst lake expansion from ref. [14] is ~0.29% yr^{-1} until 2060). However, contrary to the expectations of these models, our results show that surface water decreased more strongly in areas with high ice content than in areas with medium or low ice content ($P < 0.001$, Fig. 2). This suggests that degradation of ice-rich permafrost leads to greater increases in drainage than surface water formation and expansion.

The role of lake sedimentation

In addition to drainage, another mechanism probably contributing to permafrost thaw-driven decreases in surface water is increasing lake sedimentation, which occurs when lake-adjacent permafrost thaws and causes lake infilling[49]. This may occur rapidly and completely as a result of slope failure by abrupt thaw[49], which is often triggered by extreme heat and precipitation events[38,49,50]. Or, it may occur progressively as warmer and wetter conditions gradually increase connectivity between lakes and the surrounding land[51].

Table 2 | Trends in climate variables derived from the ERA5-Land reanalysis dataset[30] over the Eurasian and North American parts of the study region and the entire study region

	Eurasia	North America	Entire study region
Annual air temperature (°C yr^{-1})	0.12 ± 0.03	0.01 ± 0.03	0.05 ± 0.06
Annual evapotranspiration (mm yr^{-1})[a,b]	1 ± 0.69	0.42 ± 0.62	0.63 ± 0.71
Annual precipitation (mm yr^{-1})	2.14 ± 2.28	0.4 ± 2.22	1.01 ± 2.39
Autumn rain (mm yr^{-1})	0.48 ± 0.63	0.21 ± 0.93	0.3 ± 0.85
Spring rain (mm yr^{-1})	0.06 ± 0.25	0 ± 0.36	0.02 ± 0.33
Summer rain (mm yr^{-1})	0.39 ± 1.47	0.44 ± 1.55	0.42 ± 1.52
Melt water in snow (mm yr^{-1})[a]	1.23 ± 1.5	−0.79 ± 1.25	−0.11 ± 1.65
Growing season evapotranspiration (mm yr^{-1})[a,b]	0.71 ± 0.54	0.42 ± 0.56	0.52 ± 0.57
Snowmelt date (day yr^{-1})	−0.26 ± 0.32	−0.17 ± 0.28	−0.2 ± 0.3

[a]Millimetres of water equivalent. [b]The ERA5-Land reanalysis dataset uses the convention that positive values indicate condensation and negative values indicate evaporation. Here, we have reversed the sign so a positive trend in evapotranspiration indicates evapotranspiration has increased over the study period. Trends are the mean ± s.d. calculated over the period 2000–2021 for all variables except autumn rain, which is for the period 1999–2020.

Overall, our results indicate that over the past two decades, lake drainage, sedimentation and/or other mechanisms of surface water decline have exceeded surface water formation and expansion, leading to a net decrease in surface water that was not anticipated by models until ~2060 (ref. [14]) or ~2150 (ref. [20]).

Regional trends

Surface water declined more strongly in Eurasia (mean pixel-wise SWI trend of −0.001 yr^{-1}) than in North America (mean pixel-wise SWI trend of −0.0007 yr^{-1}). This regional trend may be due to several factors. First, the two most important climate predictors of surface water change (trends in autumn rain and trends in annual air temperature) increased more strongly in Eurasian than in North American areas of our study region (Table 2 and Extended Data Fig. 1). Second, the percentage of the study region with a high to very high concentration of thermokarst lakes, which on average exhibit stronger surface water declines than other land cover types (Table 1), is higher in Eurasia (60%) than in North America (15%; Extended Data Fig. 4).

Future surface water change and climate feedbacks

Our results show that, on average, surface water has declined across lake-rich regions of the Arctic in recent decades and that the most likely cause is drainage and/or sedimentation due to permafrost thaw. Similar results were obtained for the entire northern permafrost zone (lake-rich and non-lake-rich areas of the continuous and discontinuous permafrost north of 50° N; Extended Data Figs. 5 and 6). This thaw-induced decline is due to near equal contributions of increasing annual air temperatures and increasing autumn rain. These results are consistent with recent work suggesting that heat transfer by precipitation is equally important to air temperature as a driver of permafrost degradation[52] and evidence from across the Arctic that permafrost is thawing faster than anticipated[5,7]. Precipitation, however, is not included as a driver of permafrost thaw in some models of surface water change[17,53], which could partially explain why we observe net drainage earlier than projected. Indeed, models that do include precipitation as a driver of surface water change indicate that net decreases will occur nearly a century earlier than models that exclude this mechanism[14,20].

With continued climate change, Arctic air temperatures and autumn rain are expected to continue increasing[33,54], which will probably contribute to further surface water decline across the permafrost zone. Decreases in lake surface water will negatively impact human livelihood, as surface water in permafrost regions is often the only viable source of fresh water and northern communities rely on it for household use[55,56]. Decreasing surface water may also negatively impact fish, migrating birds and other wildlife that depend on northern lakes for habitat[57,58].

Changes in surface water involve important feedbacks to climate change. In permafrost regions, lake drainage can act as a negative feedback to climate change due to increased summer surface albedo[13] (replacing dark lake surfaces with more reflective bare ground and vegetation) and carbon uptake following vegetation expansion and reduced soil respiration due to permafrost aggradation in drained lake basins[19,59,60]. In contrast to drainage, surface water expansion is a positive feedback to climate change because lake initiation and expansion results in decreased albedo and increased carbon dioxide and methane emissions to the atmosphere[13,14,16,17,61]. Similarly, lakes that transition to wetlands, rather than draining or drying completely, may serve as persistent sources of methane emissions[62].

Our results show that there is high spatial variability in Arctic surface water change, including local increases in surface water within regions of net decline. On decadal timescales, the positive feedback effects of local surface water expansion may be stronger than the negative feedback effects of surface water decline because carbon released during lake initiation and expansion happens much faster than carbon uptake following vegetation regrowth in drained lake basins[17]. Thus, the net feedback to climate change depends not only on the net change in surface water but also on the gross changes and the timescale considered.

None of the Earth System Models included in recent Coupled Model Intercomparison Projects (CMIPs) include fine-scale abrupt thaw processes probably responsible for surface water drainage and lake infilling due to sedimentation[63,64]. Other types of models have been developed to study the potential effects of abrupt permafrost thaw on carbon emissions[14,17,20,65]. However, contrary to our results showing net surface water decline over the previous two decades, these models predict that surface water in the permafrost zone is currently increasing and will continue to increase until the mid-twenty-first or twenty-second centuries[14,17,20]. The observed pan-Arctic decrease in surface water in lake-rich regions and a likely trajectory towards further declines suggest that current and future estimates of carbon emissions from abrupt permafrost thaw are probably too high. A better understanding of the carbon cycle consequences of net surface water decline in the Arctic will require quantifying the carbon emissions and uptake associated with gross increases and decreases in surface water over decadal and centennial timescales.

Online content

Any methods, additional references, Nature Research reporting summaries, source data, extended data, supplementary information, acknowledgements, peer review information; details of author contributions and competing interests; and statements of data and code availability are available at https://doi.org/10.1038/s41558-022-01455-w.

Received: 16 March 2022; Accepted: 21 July 2022;
Published online: 29 August 2022

References

1. Ballinger, T. J. et al. *Surface Air Temperature* (NOAA, 2021); https://doi.org/10.25923/53xd-9k68
2. Box, J. E. et al. Key indicators of Arctic climate change: 1971-2017. *Env. Res. Lett* **14**, 045010 (2019).
3. Fujinami, H., Yasunari, T. & Watanabe, T. Trend and interannual variation in summer precipitation in eastern Siberia in recent decades. *Int. J. Climatol.* **36**, 355–368 (2016).
4. Vihma, T. et al. The atmospheric role in the Arctic water cycle: a review on processes, past and future changes, and their impacts. *J. Geophys. Res. G* **121**, 586–620 (2016).
5. Liljedahl, A. K. et al. Pan-Arctic ice-wedge degradation in warming permafrost and influence on tundra hydrology. *Nat. Geosci.* **9**, 312–318 (2016).
6. Runge, A., Nitze, I. & Grosse, G. Remote sensing annual dynamics of rapid permafrost thaw disturbances with LandTrendr. *Remote Sens. Environ.* **268**, 112752 (2022).
7. Farquharson, L. M. et al. Climate change drives widespread and rapid thermokarst development in very cold permafrost in the Canadian High Arctic. *Geophys. Res. Lett.* **46**, 6681–6689 (2019).
8. Mamet, S. D., Chun, K. P., Kershaw, G. G. L., Loranty, M. M. & Peter Kershaw, G. Recent increases in permafrost thaw rates and areal loss of palsas in the Western Northwest Territories, Canada. *Permafr. Periglac. Process.* **28**, 619–633 (2017).
9. Vasiliev, A. A. et al. Permafrost degradation in the Western Russian Arctic. *Environ. Res. Lett.* **15**, 045001 (2020).
10. Nitze, I., Grosse, G., Jones, B. M., Romanovsky, V. E. & Boike, J. Remote sensing quantifies widespread abundance of permafrost region disturbances across the Arctic and Subarctic. *Nat. Commun.* **9**, 5423 (2018).
11. Smith, L. C., Sheng, Y., MacDonald, G. M. & Hinzman, L. D. Disappearing Arctic lakes. *Science* **308**, 1429 (2005).
12. Grosse, G., Jones, B. & Arp, C. in *Treatise on Geomorphology* (eds Shroder, J. et al.) 325–353 (Academic Press, 2013).
13. Webb, E. E., Loranty, M. M. & Lichstein, J. W. Surface water, vegetation, and fire as drivers of the terrestrial Arctic-boreal albedo feedback. *Environ. Res. Lett.* **16**, 084046 (2021).
14. van Huissteden, J. et al. Methane emissions from permafrost thaw lakes limited by lake drainage. *Nat. Clim. Change* **1**, 119–123 (2011).
15. Walter, K. M., Zimov, S. A., Chanton, J. P., Verbyla, D. & Chapin, F. S. Methane bubbling from Siberian thaw lakes as a positive feedback to climate warming. *Nature* **443**, 71–75 (2006).
16. Wik, M., Varner, R. K., Anthony, K. W., MacIntyre, S. & Bastviken, D. Climate-sensitive northern lakes and ponds are critical components of methane release. *Nat. Geosci.* **9**, 99–105 (2016).
17. Walter Anthony, K. et al. 21st-century modeled permafrost carbon emissions accelerated by abrupt thaw beneath lakes. *Nat. Commun.* **9**, 3262 (2018).
18. in't Zandt, M. H., Liebner, S. & Welte, C. U. Roles of thermokarst lakes in a warming world. *Trends Microbiol.* **28**, 769–779 (2020).
19. Jones, B. M. et al. Lake and drained lake basin systems in Arctic and Boreal permafrost regions. *Nat. Rev. Earth Environ* **3**, 85–98 (2022).
20. Turetsky, M. R. et al. Carbon release through abrupt permafrost thaw. *Nat. Geosci.* **13**, 138–143 (2020).
21. Pastick, N. J. et al. Spatiotemporal remote sensing of ecosystem change and causation across Alaska. *Glob. Change Biol.* **25**, 1171–1189 (2019).
22. Carroll, M. L. & Loboda, T. V. Multi-decadal surface water dynamics in North American tundra. *Remote Sens* **9**, 497 (2017).
23. Finger Higgens, R. A. et al. Changing lake dynamics indicate a drier Arctic in Western Greenland. *J. Geophys. Res. G* **124**, 870–883 (2019).
24. Karlsson, J. M., Lyon, S. W. & Destouni, G. Temporal behavior of lake size-distribution in a thawing permafrost landscape in northwestern Siberia. *Remote Sens.* **6**, 621–636 (2014).
25. Jones, B. M. et al. Modern thermokarst lake dynamics in the continuous permafrost zone, northern Seward Peninsula, Alaska. *J. Geophys. Res. G* https://doi.org/10.1029/2011JG001666 (2011).
26. Sharma, R. C., Tateishi, R., Hara, K. & Nguyen, L. V. Developing Superfine Water Index (SWI) for global water cover mapping using MODIS data. *Remote Sens.* **7**, 13807–13841 (2015).
27. Nitze, I. et al. The catastrophic thermokarst lake drainage events of 2018 in northwestern Alaska: fast-forward into the future. *Cryosphere* **14**, 4279–4297 (2020).
28. Lara, M. J., Chen, Y. & Jones, B. M. Recent warming reverses forty-year decline in catastrophic lake drainage and hastens gradual lake drainage across northern Alaska. *Env. Res. Lett* **16**, 124019 (2021).
29. Marsh, P., Russell, M., Pohl, S., Haywood, H. & Onclin, C. Changes in thaw lake drainage in the Western Canadian Arctic from 1950 to 2000. *Hydrol. Process.* **23**, 145–158 (2009).
30. Muñoz Sabater, J. *ERA5-Land Hourly Data from 1981 to Present* (Climate Data Store, 2019); https://doi.org/10.24381/cds.e2161bac
31. Dobricic, S., Russo, S., Pozzoli, L., Wilson, J. & Vignati, E. Increasing occurrence of heat waves in the terrestrial Arctic. *Environ. Res. Lett.* **15**, 024022 (2020).
32. Rawlins, M. A. et al. Analysis of the Arctic system for freshwater cycle intensification: observations and expectations. *J. Clim.* **23**, 5715–5737 (2010).

33. McCrystall, M. R., Stroeve, J., Serreze, M., Forbes, B. C. & Screen, J. A. New climate models reveal faster and larger increases in Arctic precipitation than previously projected. *Nat. Commun.* **12**, 16765 (2021).
34. Yu, L. & Zhong, S. Trends in Arctic seasonal and extreme precipitation in recent decades. *Theor. Appl. Climatol.* **145**, 1541–1559 (2021).
35. Douglas, T. A., Turetsky, M. R. & Koven, C. D. Increased rainfall stimulates permafrost thaw across a variety of Interior Alaskan boreal ecosystems. *npj Clim. Atmos. Sci* **3**, 28 (2020).
36. Iijima, Y. et al. Abrupt increases in soil temperatures following increased precipitation in a permafrost region, central Lena River basin, Russia. *Permafr. Periglac. Process.* **21**, 30–41 (2010).
37. Romanovsky, V. E. & Osterkamp, T. E. Effects of unfrozen water on heat and mass transport processes in the active layer and permafrost. *Permafr. Periglac. Process* **11**, 219–239 (2000).
38. Kokelj, S. V. et al. Increased precipitation drives mega slump development and destabilization of ice-rich permafrost terrain, northwestern Canada. *Glob. Planet. Change* **129**, 56–68 (2015).
39. Christensen, T. R. et al. Multiple ecosystem effects of extreme weather events in the Arctic. *Ecosystems* **24**, 122–136 (2021).
40. Fortier, D., Allard, M. & Shur, Y. Observation of rapid drainage system development by thermal erosion of ice wedges on Bylot Island, Canadian Arctic Archipelago. *Permafr. Periglac. Process.* **18**, 229–243 (2007).
41. Jones, B. M. & Arp, C. D. Observing a catastrophic thermokarst lake drainage in Northern Alaska. *Permafr. Periglac. Process.* **26**, 119–128 (2015).
42. Throckmorton, H. M. et al. Active layer hydrology in an Arctic tundra ecosystem: quantifying water sources and cycling using water stable isotopes. *Hydrol. Process.* **30**, 4972–4986 (2016).
43. Swanson, D. K. Thermokarst and precipitation drive changes in the area of lakes and ponds in the National Parks of northwestern Alaska, 1984–2018. *Arct. Antarct. Alp. Res.* **51**, 265–279 (2019).
44. Connon, R. F., Quinton, W. L., Craig, J. R. & Hayashi, M. Changing hydrologic connectivity due to permafrost thaw in the lower Liard River valley, NWT, Canada. *Hydrol. Process.* **28**, 4163–4178 (2014).
45. Brewer, M. C. The thermal regime of an Arctic lake. *Eos Trans. Am. Geophys. Union* **39**, 278–284 (1958).
46. Jorgenson, M. T. et al. Resilience and vulnerability of permafrost to climate change. *Can. J. Res.* **40**, 1219–1236 (2010).
47. Yoshikawa, K. & Hinzman, L. D. Shrinking thermokarst ponds and groundwater dynamics in discontinuous permafrost near Council, Alaska. *Permafr. Periglac. Process.* **14**, 151–160 (2003).
48. Jorgenson, M. T. et al. *Permafrost Characteristics of Alaska* (University of Alaska Fairbanks, 2008); https://permafrost.gi.alaska.edu/sites/default/files/AlaskaPermafrostMap_Front_Dec2008_Jorgenson_etal_2008.pdf
49. Lewkowicz, A. G. & Way, R. G. Extremes of summer climate trigger thousands of thermokarst landslides in a High Arctic environment. *Nat. Commun.* **10**, 1329 (2019).
50. Lacelle, D., Bjornson, J. & Lauriol, B. Climatic and geomorphic factors affecting contemporary (1950–2004) activity of retrogressive thaw slumps on the Aklavik plateau, Richardson mountains, NWT, Canada. *Permafr. Periglac. Process.* **21**, 1–15 (2010).
51. Kuhn, C. & Butman, D. Declining greenness in Arctic-boreal lakes. *Proc. Natl Acad. Sci. USA* **118**, e2021219118 (2021).
52. Mekonnen, Z. A., Riley, W. J., Grant, R. F. & Romanovsky, V. E. Changes in precipitation and air temperature contribute comparably to permafrost degradation in a warmer climate. *Env. Res. Lett* **16**, 024008 (2021).
53. Schneider von Deimling, T. et al. Estimating the near-surface permafrost-carbon feedback on global warming. *Biogeosciences* **9**, 649–665 (2012).
54. Bintanja, R. & Selten, F. M. Future increases in Arctic precipitation linked to local evaporation and sea-ice retreat. *Nature* **509**, 479–482 (2014).
55. White, D. M., Craig Gerlach, S., Loring, P., Tidwell, A. C. & Chambers, M. C. Food and water security in a changing Arctic climate. *Env. Res. Lett* **2**, 045018 (2007).
56. Medeiros, A. S., Wood, P., Wesche, S. D., Bakaic, M. & Peters, J. F. Water security for northern peoples: review of threats to Arctic freshwater systems in Nunavut, Canada. *Reg. Environ. Change* **17**, 635–647 (2017).
57. Roach, J. K. & Griffith, B. Climate-induced lake drying causes heterogeneous reductions in waterfowl species richness. *Landsc. Ecol.* **30**, 1005–1022 (2015).
58. Cott, P. A., Sibley, P. K., Somers, W. M., Lilly, M. R. & Gordon, A. M. A review of water level fluctuations on aquatic biota with an emphasis on fishes in ice-covered lakes. *J. Am. Water Resour. Assoc.* **44**, 343–359 (2008).
59. Jones, M. C., Grosse, G., Jones, B. M. & Walter Anthony, K. Peat accumulation in drained thermokarst lake basins in continuous, ice-rich permafrost, northern Seward Peninsula, Alaska. *J. Geophys. Res. G* https://doi.org/10.1029/2011JG001766 (2012).
60. Sturtevant, C. S. & Oechel, W. C. Spatial variation in landscape-level CO_2 and CH_4 fluxes from Arctic coastal tundra: influence from vegetation, wetness, and the thaw lake cycle. *Glob. Change Biol.* **19**, 2853–2866 (2013).
61. Walter Anthony, K. et al. Methane emissions proportional to permafrost carbon thawed in Arctic lakes since the 1950s. *Nat. Geosci.* **9**, 679–682 (2016).
62. Kuhn, M. A. et al. BAWLD-CH4: a comprehensive dataset of methane fluxes from boreal and Arctic ecosystems. *Earth Syst. Sci. Data* **13**, 5151–5189 (2021).
63. Andresen, C. G. et al. Soil moisture and hydrology projections of the permafrost region—a model intercomparison. *Cryosphere* **14**, 445–459 (2020).
64. Burke, E. J., Zhang, Y. & Krinner, G. Evaluating permafrost physics in the Coupled Model Intercomparison Project 6 (CMIP6) models and their sensitivity to climate change. *Cryosphere* **14**, 3155–3174 (2020).
65. Tan, Z. & Zhuang, Q. Methane emissions from pan-Arctic lakes during the 21st century: an analysis with process-based models of lake evolution and biogeochemistry. *J. Geophys. Res. G* **120**, 2641–2653 (2015).
66. Olefeldt, D. Circumpolar distribution and carbon storage of thermokarst landscapes. *Nat. Commun.* **7**, 13043 (2016).
67. Brown, J., Ferrians, O., Heginbottom, J. A. & Melnikov, E. *Circum-Arctic Map of Permafrost and Ground-Ice Conditions* v.2 (NSIDC, accessed October 2021); https://doi.org/10.7265/skbg-kf16
68. Olefeldt, D. et al. The Boreal-Arctic Wetland and Lake Dataset (BAWLD). *Earth Syst. Sci. Data* **13**, 5127–5149 (2021).

Methods

General approach. To determine the drivers of surface water change (2000–2021) across the permafrost zone, we mapped (1) the pixel-wise trends in July surface water across the study region, (2) the pixel-wise trends in climate variables expected to contribute to surface water change and (3) the landscape characteristics expected to influence surface water change. We then used a machine learning approach to relate the surface water trends to the climate trends and landscape characteristics.

Study area. Our study region was the continuous and discontinuous permafrost zone north of 50° N where the percentage of surface area covered by lakes is ≥5%. The study region covered 77% of areas with high to very high (30–100%) thermokarst lake coverage, 53% of areas with low to moderate (1–30%) thermokarst lake coverage, 27% of the continuous permafrost zone and 20% of the discontinuous permafrost zone. Lakes occupy ~15% of the surface area of the study region. We limited the study area to lake-rich regions because, like all remote sensing indices, the SWI[26] (used to determine surface water trends; see below) is responsive to changes in all bands, including bands that are sensitive to non-water surfaces. Changes in the SWI in non-lake-rich regions could indicate changes in non-water surfaces, and we sought to minimize these errors by restricting our analysis to regions with high lake cover, where we assume that changes in SWI are most likely to reflect true changes in surface water. Our main conclusions were not qualitatively affected by this choice; when we included the entire continuous and discontinuous permafrost zones north of 50° N in our analysis, the results showed that surface water declined across the region, due mainly to changes in annual air temperature and autumn rain (Extended Data Figs. 5 and 6).

Within this study area, recently burned areas (details below) and pixels identified by the European Space Agency Climate Change Initiative Land Cover Maps[69] as permanent snow and ice or agricultural or urban land were omitted. While fire is known to cause permafrost thaw and changes in surface water[70,71], we excluded recently burned areas because preliminary analysis indicated that the SWI did not reliably distinguish between char and water without further optimization. Because our goal was to study changes in the area of lakes and other inland waters, rather than surface water change caused by coastal erosion and sea level rise, we also excluded land within 5 km of the coast. Permafrost extent was delineated according to ref. [67], and lake cover percentage data came from ref. [68]. Burned pixels were identified from four products: the Bureau of Land Management, Alaska Fire Service Historical Wildfires database[72], the Canadian National Fire Database[73], the MODIS burn area product[74] and a Landsat-based data product of fires in Siberia[75]. These products allowed us to exclude areas that burned in North America between 1995 and 2021 and in Eurasia between 2000 and 2021.

Surface water trends. We limited our analysis to changes in surface water during the month of July, when our study region is typically snow-free. For each 500 m pixel, we used the MODIS Nadir Bidirectional Reflectance Distribution Function-Adjusted Reflectance (NBAR) product[76] to compute the SWI[26]:

$$\mathrm{SWI} = \frac{\mathrm{Sat}_{(\mathrm{RGB})} - 7 \times \mathrm{NIR}}{\mathrm{Sat}_{(\mathrm{RGB})} + 7 \times \mathrm{NIR}} \quad (1)$$

where $\mathrm{Sat}_{(\mathrm{RGB})}$ is the hue-saturation-value transformation of the RGB composite made up of red (R), green (G) and blue (B) bands and NIR is the near infrared band. After excluding retrievals with any snow (pixels where the MODIS snow cover product[77] was greater than zero), we calculated the average July SWI ($\mathrm{SWI}_{\mathrm{July}}$) for each pixel in each year. We then quantified the pixel-wise temporal trend (or 'change') in surface water as the Sen's slope of $\mathrm{SWI}_{\mathrm{July}}$ versus year. The Sen's slope[78] is relatively insensitive to outliers and is therefore widely used to reduce the effects of random noise when estimating pixel-wise trends in large-scale geospatial datasets (for example, refs. [79,80]). To further reduce the influence of outliers, which may reflect data acquisition or processing errors, pixels with a slope >8 s.d. from the mean slope were excluded from further analysis.

Surface water trends were calculated for each MODIS pixel within the study region, and these 500 m pixels were then averaged to 12 km pixels. We chose a pixel size of 12 km because aggregation was necessary to match spatial scales between explanatory and response variables and because initial data exploration revealed that the model R^2 was highest when pixels were aggregated to 12 km. All subsequent analyses were based on the aggregated 12 km pixels, except for analysis of spatial variability (Table 1), which used the original 500 m pixels.

Climate trends and landscape characteristics. We explored different climate and landscape variables as potential drivers of surface water trends. Climate variables included in our analysis were the pixel-wise trends in spring, summer, autumn and total growing season rain accumulation; autumn, winter and spring snow accumulation; spring, summer, autumn, winter and annual temperature means; growing season evapotranspiration; water in snowmelt (January–July); snow onset date; and snowmelt date. For all variables, we used the following seasonal definitions: spring—March, April, May; summer—June, July, August; autumn—September, October, November; winter—December, January, February; growing season—June–September. For the rain, snow, melt water and evapotranspiration variables, we first summed the daily accumulation values for each season ($\mathrm{Variable}_{\mathrm{sum}}$) and then quantified the Sen's slope of $\mathrm{Variable}_{\mathrm{sum}}$ versus year. For the temperature variables, we first took the seasonal average hourly air temperature at 2 m ($\mathrm{Variable}_{\mathrm{mean}}$) and then quantified the Sen's slope of $\mathrm{Variable}_{\mathrm{mean}}$ versus year. Snowmelt and onset dates were defined as the first and last day of the calendar year with zero per cent snow cover ($\mathrm{DOY}_{\mathrm{zero}}$), and their trends were quantified as the Sen's slope of $\mathrm{DOY}_{\mathrm{zero}}$ versus year. Autumn trends were calculated over the period 1999–2020, snow onset was calculated for 2000–2020 and all other trends were calculated over the period 2000–2021. We defined the winter of year x as the December of year $x-1$ and January and February of year x.

Rain, snow, melt water, evapotranspiration and air temperature data were obtained from the ERA5-Land reanalysis dataset[30]. For evapotranspiration, we use the variable 'total_evaporation' in the ERA5-Land reanalysis because it includes a simplified representation of transpiration in addition to evaporation. Snow cover data came from the MODIS snow cover product[77]. The temporal trend in each variable was calculated in its native resolution and then averaged to 12 km pixels.

We included the following landscape characteristics in our analysis: ground ice content[67], permafrost designation[67], overburden thickness[67], the percentage of surface area covered by lakes[68] and land cover type[68]. These categorical variables were converted from vector to raster format, using the same 12 km pixels as the continuous variables. We performed an analysis of variance (ANOVA) and Tukey's Honest Significant Different test to determine if surface water trends were significantly different between permafrost zones and between areas with varying amounts of ice content. To determine if lake type impacted surface water trends, we fit nested linear regression models of surface water change with the percentage cover of lake types in each 12 km pixel as explanatory variables. The explanatory variables in the nested models were (1) the percentage cover of all lake types combined, (2) the percentage cover of yedoma and peat lakes combined and the percentage cover of glacial lakes and (3) the percentage cover of each lake type. We then performed an ANOVA on the models to determine the best fit model.

Quantifying the drivers of surface water change. To quantify the effects of the potential drivers of surface water trends, we fit a histogram-based gradient boosting regression tree (HGBRT) model that related trends in surface water to landscape characteristics and trends in climate variables. To focus on pixels where surface water change is substantial, we restricted this analysis to pixels whose surface water trends were in the lower/upper 20th/80th percentile of the 12 km pixels. We chose the HGBRT approach because regression trees are an easily interpretable method of determining variable importance and ensemble methods such as boosting generally produce better models (lower bias and variance) than single tree methods[81]. We fit the HGBRT using the Python-based Scikit-learn library[82], and optimal model hyperparameters were determined using grid search and tenfold cross validation[81,83].

Preliminary analyses revealed that collinearity among some explanatory variables complicated model inference (the estimated importance of some variables changed considerably when other variables were included in the model). To overcome this issue, we calculated the Pearson's correlation coefficient (r) between all variables. We then removed variables that were highly correlated ($r > 0.5$) with variables that were the most important to model performance in preliminary analyses (see methods on variable importance below). Variables omitted for this reason include snow onset, overburden thickness, snow accumulation, permafrost designation (continuous versus discontinuous) and land cover type.

The model performed better (resulted in a higher R^2 value) when rain accumulation was partitioned seasonally (spring, summer and autumn rain were included individually rather than as total growing season rain) and when mean annual temperature was included rather than the seasonal temperature means. As a result, annual rain and seasonal temperature variables were removed from the model. The final model included lake percentage cover, ground ice and trends in annual air temperature, autumn rain, spring rain, melt water in snow, summer rain, evapotranspiration and snowmelt date. The final model R^2 was 0.57.

We used two methods to assess the relative importance of each explanatory variable: permutation importance and Shapley values. Permutation importance randomly shuffles the value of each explanatory variable among all pixels many times and reports the resulting drop in average R^2 value. Shapley values quantify the contribution of each explanatory variable to the predicted value of the response variable. Thus, both metrics seek to quantify a variable's contribution to explaining variation in the response but using different approaches. We compared both metrics to evaluate if our inferences regarding the importance of different explanatory variables are robust. We calculated permutation importance with 100 permutations using the Scikit-learn implementation[82] and Shapley values using the SHAP library[84]. To put the two measures of variable importance on a common scale, we calculated the relative importance of each variable by dividing its importance value by the importance value of the most important variable.

Data availability

The analysis in this study relied on datasets from the following sources, all of which are freely available to the public. The climate trends were generated using Copernicus Climate Change Service Information [2022] ERA5-Land hourly data (2 m temperature, total evaporation, snowmelt, snowfall and total precipitation) (https://cds.climate.copernicus.eu/cdsapp#!/dataset/10.24381/cds.e2161bac?tab=overview). The surface water trends were generated using the MODIS MCD43A4.006 product (https://doi.org/10.5067/MODIS/MCD43A4.006). Snow cover trends were generated using the MODIS MOD10A1.006 product (https://doi.org/10.5067/MODIS/MOD10A1.006). Fire masking was based on MODIS MCD64A1.006 (https://doi.org/10.5067/MODIS/MCD64A1.006), fire perimeters for eastern Siberia taiga and tundra (https://arcticdata.io/catalog/view/doi%3A10.18739%2FA2N87311N), the Canadian National Forest Service National Fire Database fire perimeters (http://cwfis.cfs.nrcan.gc.ca/datamart/metadata/nfdbpoly) and the Alaska Interagency Coordination Center Wildland Fire Maps (https://fire.ak.blm.gov/predsvcs/maps.php). Land cover masking was based on the ESA CCI land cover 2015 product (https://www.esa-landcover-cci.org/?q=node/164). Permafrost extent, ground cover content and overburden thickness data were from the Circum-Arctic Map of Permafrost and Ground-Ice Conditions v.2 (https://doi.org/10.7265/skbg-kf16). Lake cover percentage was from the Boreal-Arctic Wetland and Lake dataset (https://arcticdata.io/catalog/view/doi:10.18739/A2C824F9X). Thermokarst lake and thermokarst wetland coverage was from the Arctic Circumpolar Distribution and Soil Carbon of Thermokarst Landscapes dataset (https://doi.org/10.3334/ORNLDAAC/1332). Surface water trends generated for this study are archived through the Arctic Data Center (https://doi.org/10.18739/A2037V). Source data are provided with this paper.

Code availability
Google Earth Engine code used to calculate surface water and climate variable trends and Python code used to perform machine learning analysis are available on GitHub (https://github.com/webb-e/Pan-Arctic-SWchange).

References

69. Defourny, P. ESA Land Cover Climate Change Initiative (Land_Cover_cci): Global Land Cover Maps v.2.0 (ESA, 2017).
70. Jones, B. M. et al. Recent Arctic tundra fire initiates widespread thermokarst development. *Sci. Rep.* **5**, 15865 (2015).
71. Travers-Smith, H. Z., Lantz, T. C. & Fraser, R. H. Surface water dynamics and rapid lake drainage in the Western Canadian Subarctic (1985–2020). *J. Geophys. Res. G* **126**, e2021 (2021).
72. *Alaska Fire History Perimeter Polygons* (Alaska Interagency Coordination Center, 2021); https://fire.ak.blm.gov/content/maps/aicc/Data/Data%20(zipped%20filegeodatabases)/AlaskaFireHistoryPerimeters_NWCG_AICC_1940_2021.zip
73. *National Fire Database—Agency Provided Fire Perimeters* (Canadian National Forest Service, 2019); http://cwfis.cfs.nrcan.gc.ca/datamart/metadata/nfdbpoly
74. Giglio, L., Justice, C., Boschetti, L. & Roy, D. *MCD64A1 MODIS/Terra+Aqua Burned Area Monthly L3 Global 500 m SIN Grid V006* [Data set] (NASA EOSDIS Land Processes DAAC, 2015); https://doi.org/10.5067/MODIS/MCD64A1.006
75. Talucci, A. C., Loranty, M. M. & Alexander, H. D. Siberian taiga and tundra fire regimes from 2001–2020. *Environ. Res. Lett.* **17**, 025001 (2022).
76. Schaaf, C. & Wang, Z. *MCD43A4 MODIS/Terra+Aqua BRDF/Albedo Nadir BRDF Adjusted Ref Daily L3 Global 500 m V006* [Data set] (NASA EOSDIS Land Processes DAAC, 2015); https://doi.org/10.5067/MODIS/MCD43A4.006
77. Hall, D. K. & Riggs, G. A. *MODIS/Aqua Snow Cover Dly. L3 Glob. 500 m. SIN Grid, Version 6 (MYD10AI)* [Data set] (NASA National Snow and Ice Data Center Distributed Active Archive Center, 2016); https://doi.org/10.5067/MODIS/MYD10A1.006
78. Sen, P. K. Estimates of the regression coefficient based on Kendall's Tau. *J. Am. Stat. Assoc.* **63**, 1379–1389 (1968).
79. Chen, C., He, B., Yuan, W., Guo, L. & Zhang, Y. Increasing interannual variability of global vegetation greenness. *Env. Res. Lett.* **14**, 124005 (2019).
80. Guay, K. C. et al. Vegetation productivity patterns at high northern latitudes: a multi-sensor satellite data assessment. *Glob. Change Biol.* **20**, 3147–3158 (2014).
81. Elith, J., Leathwick, J. R. & Hastie, T. A working guide to boosted regression trees. *J. Anim. Ecol.* **77**, 802–813 (2008).
82. Pedregosa, F. et al. Scikit-learn: machine learning in Python. *J. Mach. Learn. Res.* **12**, 2825–2830 (2011).
83. Kohavi, R. A study of cross-validation and bootstrap for accuracy estimation and model selection. In *Proc. 14th International Joint Conference on Artificial Intelligence* Vol. 2 1137–1143 (Morgan Kaufmann, 1995).
84. Lundberg, S. M. et al. From local explanations to global understanding with explainable AI for trees. *Nat. Mach. Intell.* **2**, 56–67 (2020).

Acknowledgements
This work was supported by NASA FINESST Award 80NSSC19K134 to E.W. and J.L., NSF Awards OPP-1722572/OPP-2051888 to A.L. and NSF awards RISE-1927872/ICER-1927723/ICER-2052107 to A.L. and C.W.

Author contributions
E.W. developed the concept and designed the analysis with assistance from A.L., M.L. and J.L. E.W. performed the main-text analyses. J.C. and C.W. assisted with validation analyses. E.W. wrote the manuscript with assistance from J.L. and all authors edited the manuscript.

Competing interests
The authors declare no competing interests.

Additional information
Extended data is available for this paper at https://doi.org/10.1038/s41558-022-01455-w.

Supplementary information The online version contains supplementary material available at https://doi.org/10.1038/s41558-022-01455-w.

Correspondence and requests for materials should be addressed to Elizabeth E. Webb.

Peer review information *Nature Climate Change* thanks Rebecca Finger-Higgens, J. (Ko) van Huissteden and the other, anonymous, reviewer(s) for their contribution to the peer review of this work.

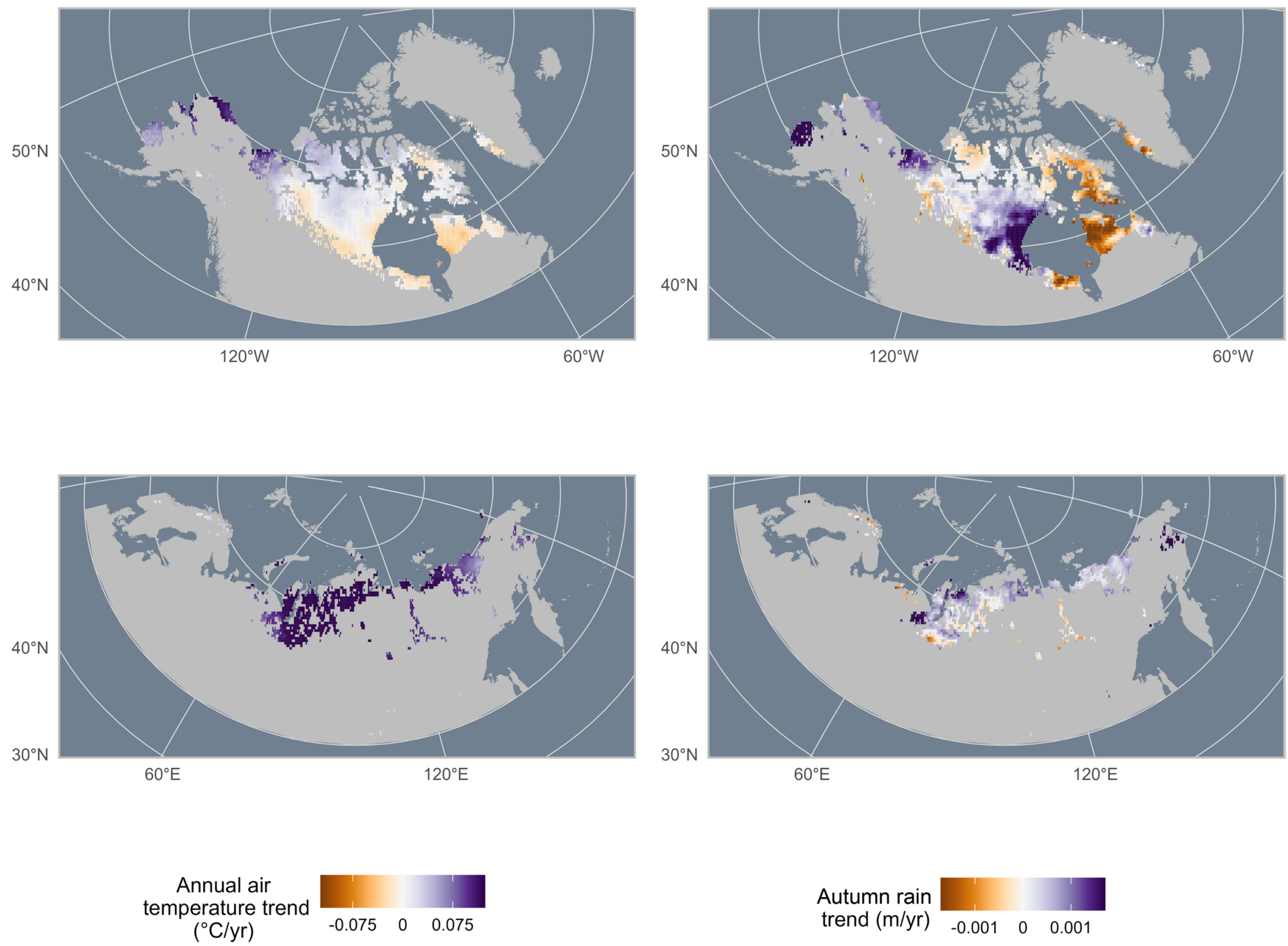

Extended Data Fig. 1 | Trends in annual air temperature and fall rain across the study region. Trends are derived from the ERA5-Land reanalysis dataset[30] for 2000–2021 (annual air temperature) and 1999–2020 (autumn rain). Generated using Copernicus Climate Change Service Information [2022].

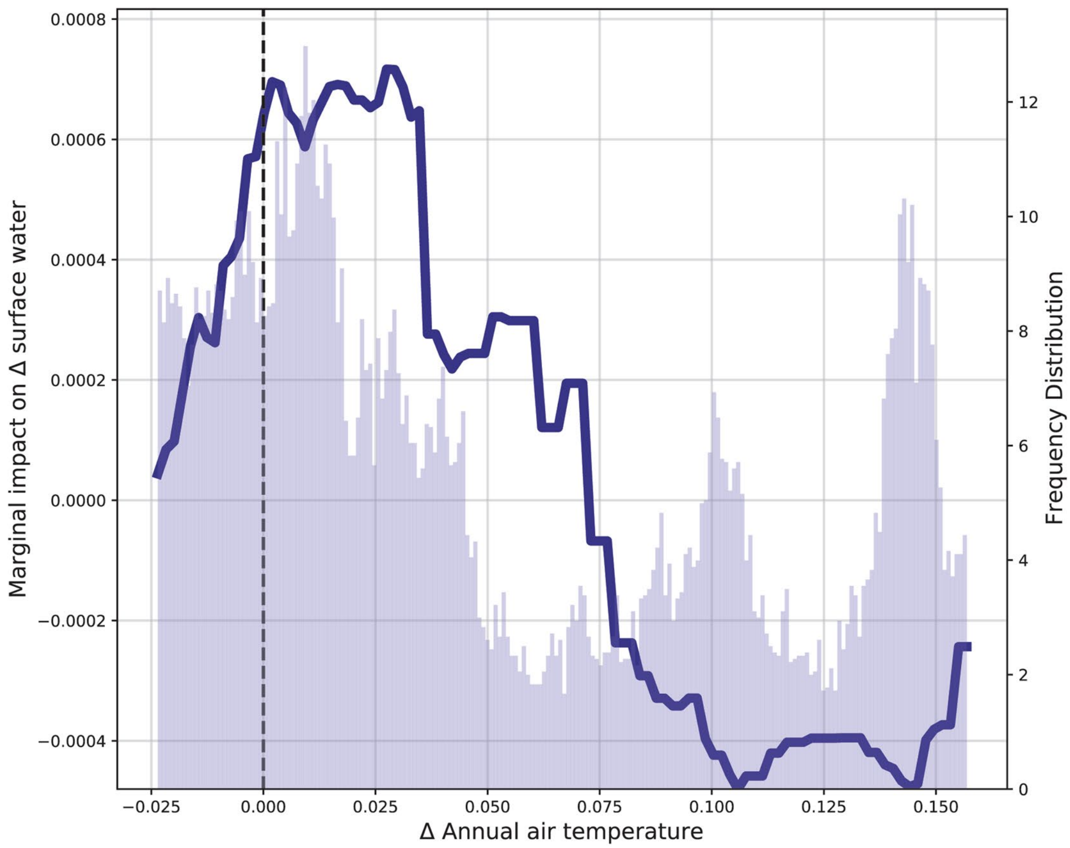

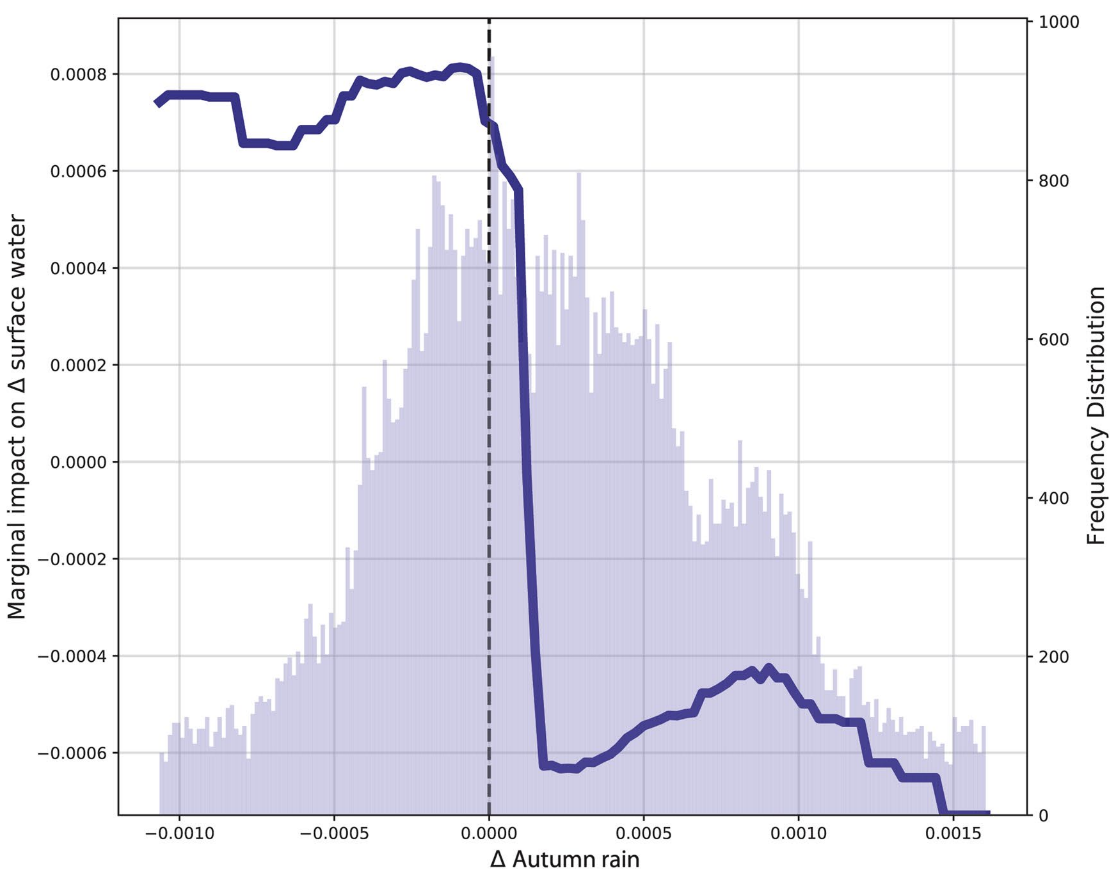

Extended Data Fig. 2 | Partial dependence plots for the effect of annual temperature trends and autumn rain trends on surface water trends. These plots show that after controlling for variation in other predictors, increasing annual temperature and increasing autumn rain both lead to decreases in surface water at a given location. The line shows the partial dependence relationships, and the histogram shows the frequency distribution of 12 km pixels.

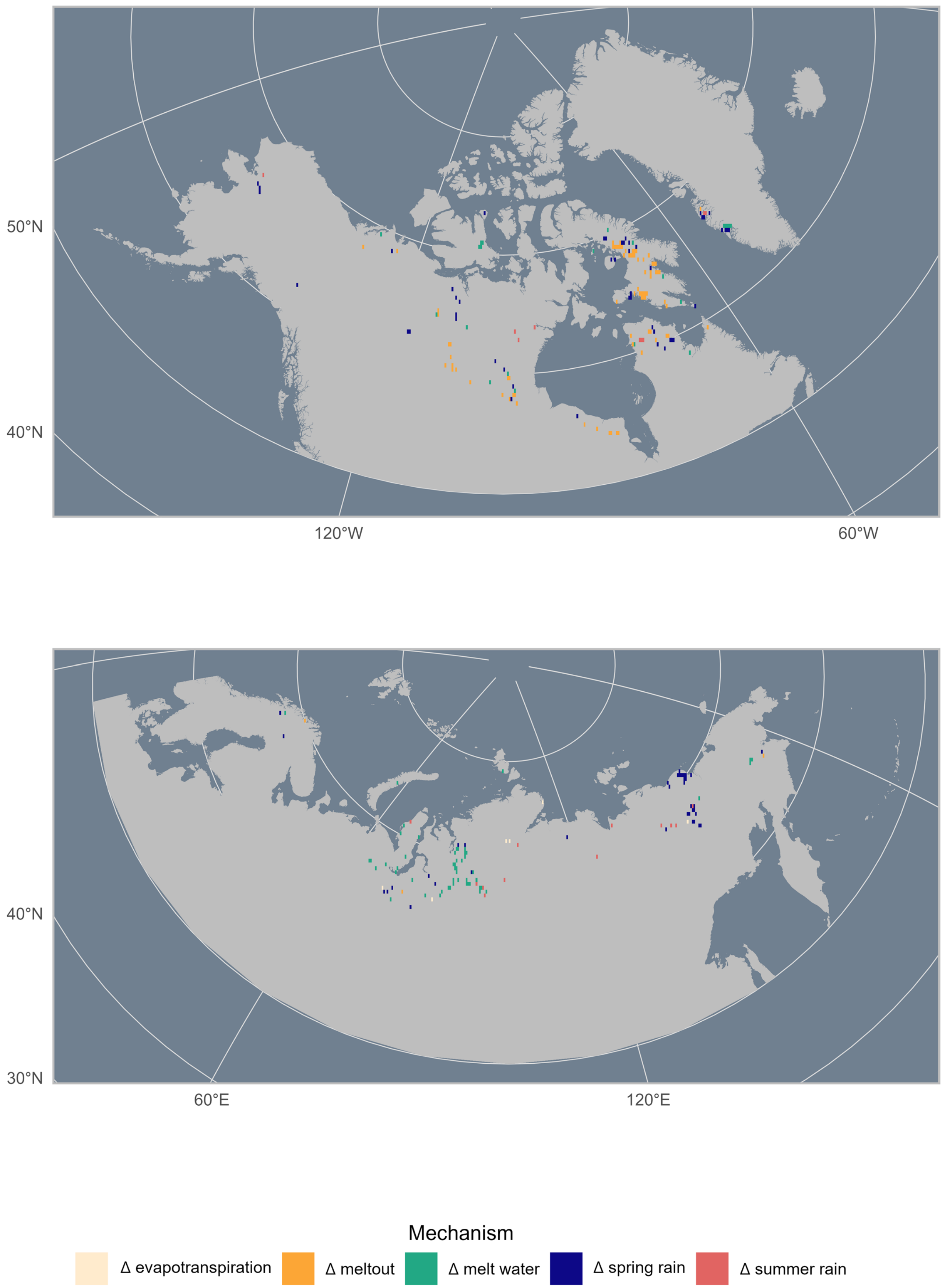

Extended Data Fig. 3 | Predictor variables, other than changes in annual air temperature and autumn rain, contributing the most to surface water trends, as determined using Shapley values. Pixels in this figure are marked as 'other' in Fig. 4.

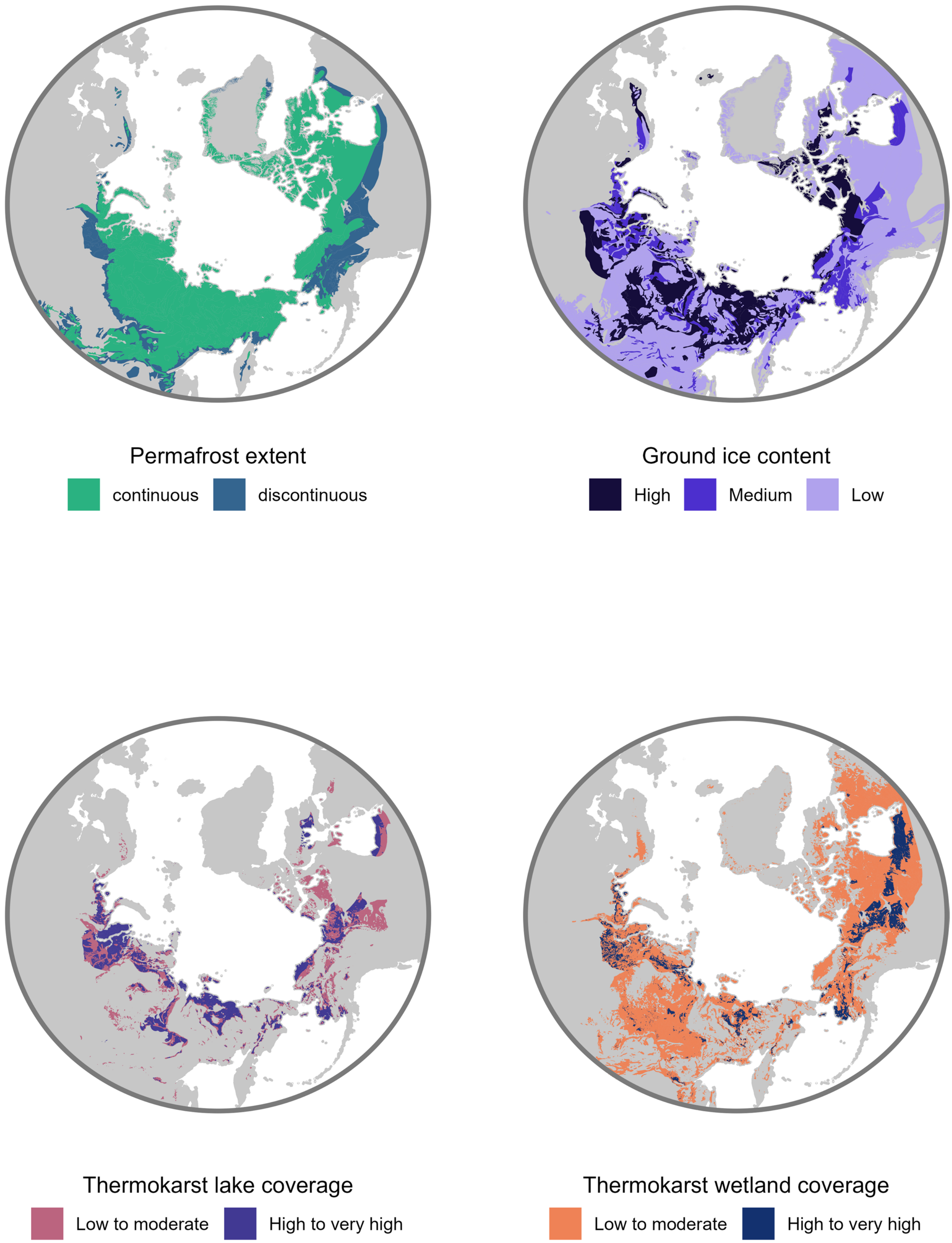

Extended Data Fig. 4 | Circumpolar distribution of continuous and discontinuous permafrost extent, ground ice content, thermokarst lake coverage, and thermokarst wetland coverage. 'High to very high' and 'low to moderate' indicate fractional coverage of wetlands and lakes (high to very high: 30–100%; low to moderate: 1–30%). Permafrost extent and ground ice content is from ref. [67] and thermokarst lake and wetland coverage is from ref. [66].

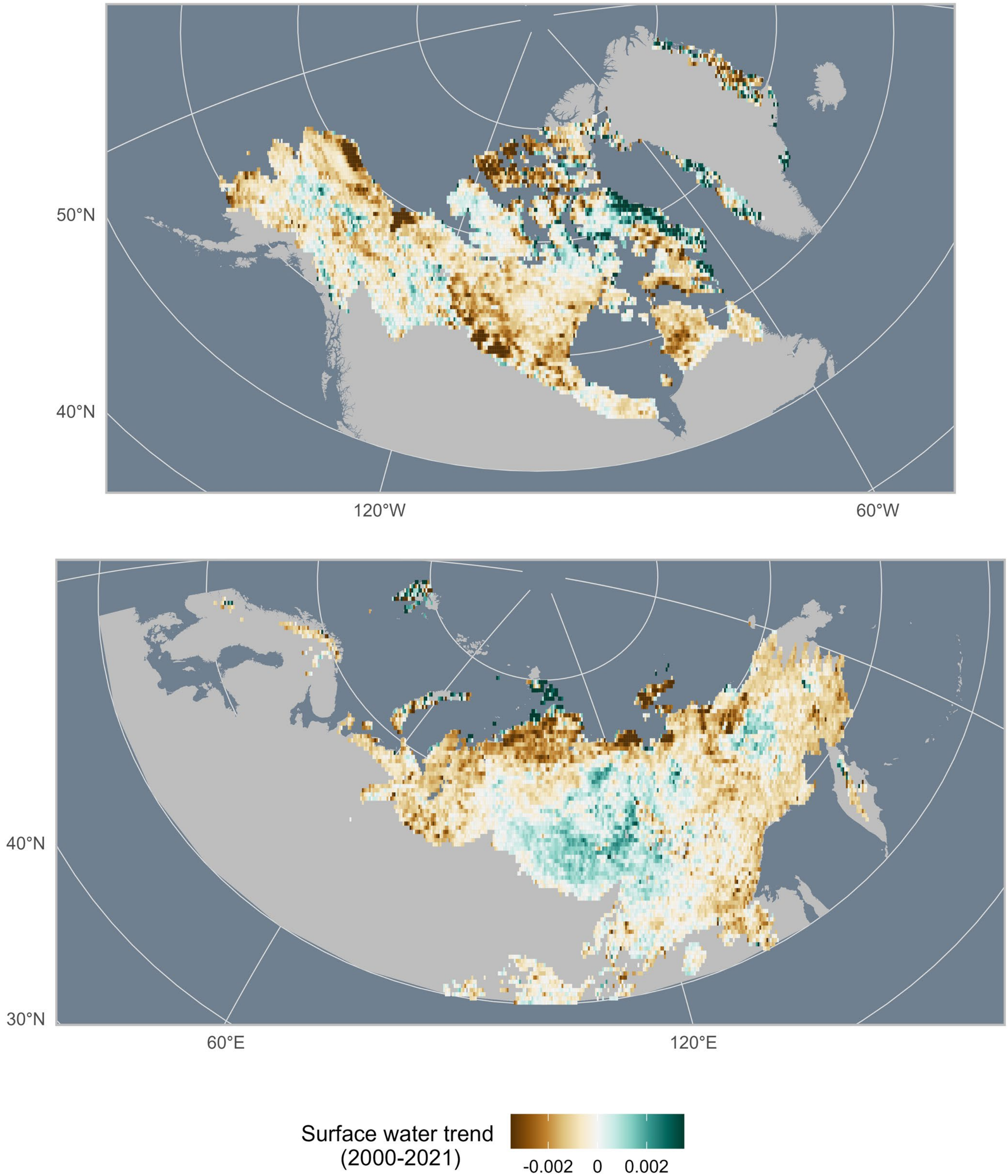

Extended Data Fig. 5 | Change in the average July superfine water index (yr[-1]) from 2000 to 2021 across the entire northern permafrost zone. As in Fig. 1, but trends are calculated over the entire northern permafrost region (lake-rich and non-lake-rich areas of the continuous and discontinuous permafrost north of 50° N) rather than only in lake-rich regions.

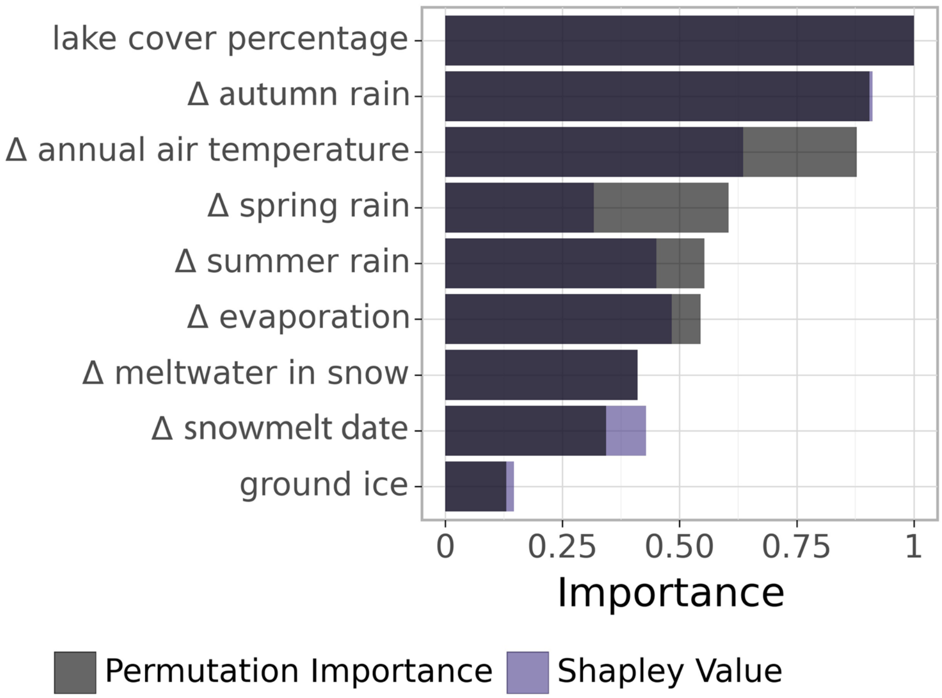

Extended Data Fig. 6 | Relative importance of predictor variables in explaining surface water trends across the entire northern permafrost zone. As in Fig. 3, but relative importance is calculated based on trends and geospatial data from across the entire northern permafrost region (lake-rich and non-lake-rich areas of the continuous and discontinuous permafrost north of 50° N) rather than only in lake-rich regions.